ENCLOSURE 5

MFN 09-552

NEDO-33173, Supplement 2, Part 2

Non-Proprietary Version

IMPORTANT NOTICE

This is a non-proprietary version of NEDC-33173P, Supplement 2, Part 2, from which the proprietary information has been removed. Portions of the enclosure that have been removed are indicated by an open and closed bracket as shown here [[ ]]

HITACHI

GE Hitachi Nuclear Energy

NEDO-33173
Supplement 2 Part 2
Revision 0
Class I
DRF 0000-0012-1297
DRF Section 0000-0103-8228-R0
August 2009

Non-Proprietary Information

Licensing Topical Report

Applicability of GE Methods to Expanded Operating Domains –

Pin-by-Pin Gamma Scan at FitzPatrick October 2006

INFORMATION NOTICE

This is a non-proprietary version of the document NEDC-33173P, Supplement 2, Part 2, which has the proprietary information removed. Portions of the document that have been removed are indicated by an open and closed bracket as shown here [[ ]].

IMPORTANT NOTICE REGARDING THE CONTENTS OF THIS REPORT

Please Read Carefully

The information contained in this document is furnished for the purpose(s) of obtaining NRC approval of the "Applicability of GE Methods to Expanded Operating Domains - Revision 2." The only undertakings of GEH with respect to information in this document are contained in contracts between GEH and participating utilities, and nothing contained in this document shall be construed as changing those contracts. The use of this information by anyone other than those participating entities and for any purposes other than those for which it is intended is not authorized; and with respect to any unauthorized use, GEH makes no representation or warranty, and assumes no liability as to the completeness, accuracy, or usefulness of the information contained in this document.

TABLE OF CONTENTS

LIST OF FIGURES

LIST OF TABLES

Abbreviations and Acronyms List

Term	Definition
BAZ	Bottom of the Active (Fuel) Zone
BOC	Beginning of Cycle
BOP	Balance of Plant
BTU	British Thermal Unit
BWR	Boiling Water Reactor
CFR	Code of Federal Regulations
CPR	Critical Power Ratio
CR	Control Rod
EOC	End of Cycle
Exp	Exposure
FW	Feedwater
GE	General Electric Company
GEH	GE Hitachi Nuclear Energy
GENE	GE Nuclear Energy
GETAB	General Electric Thermal Analysis Basis
GNF	Global Nuclear Fuel
LHGR	Linear Heat Generation Rate
LPRM	Local Power Range Monitor
LTR	Licensing Topical Report
MAPLHGR	Maximum Average Planar Linear Head Generation Rate
MAPRAT	Maximum Average Planar Ratio
MCPR	Minimum Critical Power Ratio
Meas	Measured
MLHGR	Maximum Linear Heat Generation Rate
MOC	Middle of Cycle
NN	Narrow-Narrow (Corner of the fuel lattice most distant from control rod)
NRC	Nuclear Regulatory Commission (USA)
OLMCPR	Operating Limit Minimum Critical Power Ratio
OLMLHGR	Operating Limit Minimum Linear Heat Generation Rate
RMS	Root Mean Square
RPS	Reactor Protection System
RTP	Rated Thermal Power
S.E.	Safety Evaluation
SLMCPR	Safety Limit Minimum Critical Power Ratio
SRSS	Square Root of the Sum of Squares
TIP	Traversing In-core Probe
USNRC	United States Nuclear Regulatory Commission
Wt	Weight
WW	Wide-Wide (Closest corner of the fuel lattice to the control rod)

ABSTRACT

Gamma scan is a non-destructive method to determine the relative fission product inventory in nuclear fuel. A pin-by-pin gamma scan on two GE14 10x10 fuel assemblies was completed in 2006 at the James A. FitzPatrick nuclear power station. The agreement between the measurements and predictions using the TGBLA06 lattice physics code and the PANAC11 BWR core simulator is excellent, with pin-by-pin RMS errors less than [[ ]]. The data validate the applicability of lattice power distribution uncertainties for modern BWR core and fuel designs, as well as for current operational strategies.

1. INTRODUCTION

1.1 OVERVIEW

Power distribution validation data for operating boiling water reactors is routinely taken in the form of traversing in-core probe (TIP) measurements. In this case, the average power of the four bundles surrounding the instrument tube is detected via a neutron sensitive or gamma sensitive detector. For potentially greater resolution and at greater effort and cost, gamma scanning is an independent, non-destructive method to determine the relative fission product inventory in nuclear fuel. Gamma scan measurements for the purpose of power distribution validation may be made on either bundle average or pin-by-pin measurements.

The subject of this document is pin-by-pin gamma scan measurements made at the FitzParick nuclear power station in October of 2006 at the end of cycle 17 (EOC17). Two bundles were scanned. The first, JLM420, was a GE14 once-burnt fuel assembly originally loaded at beginning of Cycle 17 (BOC17). The second, JLD505, was a twice-burnt GE14 fuel assembly, originally loaded at BOC16. For each bundle, the bundle upper tie plate was removed and individual fuel pins transferred to the water submersible gamma spectrometer located in the spent fuel pool for measurement. The fuel assembly was then reassembled. Subsequently, the once-burnt GE14 bundle, JLM420, was re-loaded into the core during the outage.

The comparison of the data obtained from these gamma scans with GNF methods show that the differences are well within the uncertainties employed in the determination of the BWR SLMCPR.

1.2 GAMMA SCAN MEASUREMENTS

Gamma scan programs vary by specification of the physical locality of the measurement, time of performing the measurement, measuring time, and number of measurements. For example, the technique for measurements of "power" calls for detection of the 1.6 MeV gamma ray that accompanies beta decay of ^{140}La with a half-life of 40.2 hours. ^{140}La accumulates in fuel mainly from the beta decay of the fission product ^{140}Ba that has a half-life of 12.8 days. After about 10 days following reactor shutdown, ^{140}La atom density is proportional to the ^{140}Ba atom density and decays with the ^{140}Ba half-life. The ^{140}Ba distribution in fuel is characteristic of the fission distribution or integrated power history over the last 5 half-lives, or approximately 60-120 days of reactor operation.

Thus, the scan results can be used to determine "recent" core power distribution. The 12.8 day half-life of ^{140}Ba also makes it imperative that the gamma scan data be collected as soon as possible after core shutdown, usually during refueling operations, since bundles with powers of interest are normally reinserted for additional use. Spectral lines from other isotopes may be measured using specific techniques and target fuel conditions for the determination of plenum fission gas (^{85}Kr) and/or fuel exposure (^{137}Cs/^{144}Pr). However, power comparisons are the sole subject of this report.

1.3 ANALYSIS / COMPARISONS

A follow-on comparison of the measured ^{140}Ba distribution with predictions using the analytical tools of GNF (i.e., TGBLA/PANACEA) constitute a validation of methods that may be used for methods licensing or determination of other licensing uncertainties. The "Improved Steady-State Methods," also known as TGBLA06 / PANAC11, for core design, licensing, and core monitoring (Reference [1]) are the current GNF methods; this methodology is examined in this report.

The general procedure used to compare to the measured gamma scan data include the following elements. First, the power/flow history of the core is input to the nodal simulator. During this process, the TIP predictions from the core tracking may be compared to the measured TIP response for the first phase of the power distribution validation process. The second step is to integrate the power history over the last 60-120 days of operation to generate the predicted nodal relative and pin-by-pin ^{140}Ba concentrations.

The final step is to statistically compare the experimental and predicted ^{140}Ba predictions and explain the relationships on a bundle, nodal, and statistical basis. This process may also be repeated using the measured 6 inch average TIP readings that may be input to the adaptive methodology described in References [2] and [3] for consistent confirmation of SLMCPR uncertainties.

1.4 NOMENCLATURE FOR ANALYSIS APPROACHES

This document provides summaries of the comparisons of design calculations of ^{140}Ba with measured ^{140}La as a means of demonstrating the GNF capabilities for calculating nodal pin powers. There are three analytic approaches summarized herein for predicting the pin-by-pin ^{140}Ba. These three approaches are:

- The standard off-line TGBLA06 / PANAC11 non-adapted models used in GNF applications for reload design and licensing (referred to as "**off-line"**);
- The standard on-line TGBLA06 / PANAC11 application used in 3DMonicore™ with TIP and LPRM shape adaptation for on-line monitoring. The on-line process can be re-run off-line by supplying the TIP and LPRM data that allows the adaptation process to be re-created off-line (referred to as "**adapted off-line**"); and also
- The use of the lattice code TGBLA06 for nodal depletions, where the operating conditions provided as inputs to the lattice code are derived from the off-line non-adapted (referred to as "**nodal depletion**").

2. PLANT AND FUEL DESCRIPTION

Entergy Corporation's 852 MWe James A. FitzPatrick nuclear power station, which entered service in 1976, is located on the shore of Lake Ontario in the town of Scriba in Oswego County, about 90 miles east of Rochester, New York.

The FitzPatrick reactor is a high power density (51.2 kW/l) D-Lattice BWR/4 with 560 fuel assemblies that operated at 100% of the current licensed thermal power for most of Cycles 16 and 17, using a power coast-down for cycle extension at the end of both cycles. The original licensed power level was 2436 MWt; the current licensed power level is 2536 MWt, a 4.1% increase. The cycle 16 core was composed of a fairly homogeneous loading of GE12 and GE14 fuel assemblies. These GE 10x10 product lines include part length rods. The reload fuel assemblies in Cycle 17 were 10x10 GE14 product line, replacing more of the 10x10 GE12 fuel assemblies.

2.1 BUNDLES JLM420 AND JLD505 CORE LOCATIONS

Table 2.1-1 summarizes general information regarding the two bundles that were disassembled, gamma scanned, and then reassembled. The once-burnt bundle JLM420 was reinserted into the core at the completion of the gamma scan measurements.

More information regarding the bundle designs for these bundles is provided in the following two sub-sections.

Table 2.1-1

Bundle Locations in Cycles 16 and 17

Bundle ID	IAT Type	Bundle Name	Cycle 16 Location Site Coordinates	Cycle 16 Location PANACEA Coordinates	EOC16 Exposure GWd/ST	EOC16 Exposure GWd/MT
JLD505	19	[[ ]]	[23-38]	(12,8)	19.4	21.38
Bundle ID	IAT Type	Bundle Name	Cycle 17 Location Site Coordinates	Cycle 17 Location PANACEA Coordinates	EOC17 Exposure GWd/ST	EOC17 Exposure GWd/MT
JLM420	1	[[	[11-22]	(06,16)	20.42	22.51
JLD505	19	]]	[25-32]	(13,11)	38.1	42.00

2.2 DESCRIPTIONS OF BUNDLES

[[

]]

Figure 2.1-1. Description of Bundle 2794 – JLM420

[[

]]

Figure 2.2-1. Description of Bundle 2562 – JLD505

2.3 CYCLE 16 OPERATION

Cycle 16 started on 10/30/2002 and ended 09/24/2004. The inventory of fuel in the core is provided in Table 2.3-1. The location of bundle JLD505 in Cycle 16 is provided in Figure 2.3-1. A series of 79 off-line core-tracking cases deplete the core to the cycle average exposure of 14,994.87 MWd/ST at End of Cycle 16 (EOC16). At the end of the cycle, there were two blades at notch 00, and two at notch 16. These control blades were located asymmetrically in the core. Figure 2.3-2 provides the power and flow conditions for Cycle 16.

Table 2.3-1

Bundle Inventory Cycle 16

Bundle Name	IAT	# in Core	#Fresh	Avg Exp GWd/ST
[[	13	2	0	27.40
	14	82	0	31.59
	15	84	0	31.91
	16	56	0	18.33
	17	132	0	18.18
	18	8	0	13.93
	19	120	120	0.00
]]	20	76	76	0.00
	Total	560	0	15.83

	1	2	3	4	5	6	7	8	9	10	11	12	13	14	15	16	17	18	19	20	21	22	23	24	25	26	
1									14	15	15	14	14	14	14	15	15	14									52
2			Bundle IAT					15	14	16	14	16	17	17	16	14	16	15	15								50
3					15	15	15	13	17	17	17	17	14	14	17	17	17	17	14	15	15	14					48
4				15	15	16	17	18	20	20	20	20	17	17	20	20	20	20	18	17	16	15	15				46
5			14	15	17	17	20	20	20	17	20	17	19	19	17	20	17	20	20	20	17	17	15	14			44
6			15	16	17	20	17	20	16	19	16	19	14	14	19	16	19	16	20	17	20	17	16	15			42
7			15	17	20	17	19	15	19	16	19	17	19	19	17	19	16	19	15	19	17	20	17	15			40
8		15	14	18	20	20	15	19	16	19	14	19	17	17	19	14	19	16	19	15	20	20	18	14	15		38
9	14	15	17	20	20	16	19	16	19	14	19	17	19	19	17	19	14	19	16	19	16	20	20	17	15	14	36
10	15	16	17	20	17	19	16	19	14	19	17	19	15	15	19	17	19	14	19	16	19	17	20	17	16	15	34
11	15	14	17	20	20	16	19	14	19	17	19	15	19	19	15	19	17	19	14	19	16	20	20	17	14	15	32
12	14	16	17	20	17	19	17	19	17	19	15	19	17	17	19	15	19	17	19	17	19	17	20	17	16	14	30
13	14	17	14	17	19	14	19	17	19	15	19	17	14	14	17	19	15	19	17	19	14	19	17	14	17	14	28
14	14	17	14	17	19	14	19	17	19	15	19	17	14	14	17	19	15	19	17	19	14	19	17	14	17	14	26
15	14	16	17	20	17	19	17	19	17	19	15	19	17	17	19	15	19	17	19	17	19	17	20	17	16	14	24
16	15	14	17	20	20	16	19	14	19	17	19	15	19	19	15	19	17	19	14	19	16	20	20	17	14	15	22
17	15	16	17	20	17	19	16	19	14	19	17	19	15	15	19	17	19	14	19	16	19	17	20	17	16	15	20
18	14	15	17	20	20	16	19	16	19	14	19	17	19	19	17	19	14	19	16	19	16	20	20	17	15	14	18
19		15	14	18	20	20	15	19	16	19	14	19	17	17	19	14	19	16	19	15	20	20	18	14	15		16
20			15	17	20	17	19	15	19	16	19	17	19	19	17	19	16	19	15	19	17	20	17	15			14
21			15	16	17	20	17	20	16	19	16	19	14	14	19	16	19	16	20	17	20	17	16	15			12
22			14	15	17	17	20	20	20	17	20	17	19	19	17	20	17	20	20	20	17	17	15	14			10
23				15	15	16	17	18	20	20	20	20	17	17	20	20	20	20	18	17	16	15	15				08
24					14	15	15	14	17	17	17	17	14	14	17	17	17	17	13	15	15	15					06
25								15	15	16	14	16	17	17	16	14	16	14	15								04
26									14	15	15	14	14	14	14	15	15	14									02
	1	3	5	7	9	11	13	15	17	19	21	23	25	27	29	31	33	35	37	39	41	43	45	47	49	51	

Figure 2.3-1. Core Bundle Type Map Cycle 16

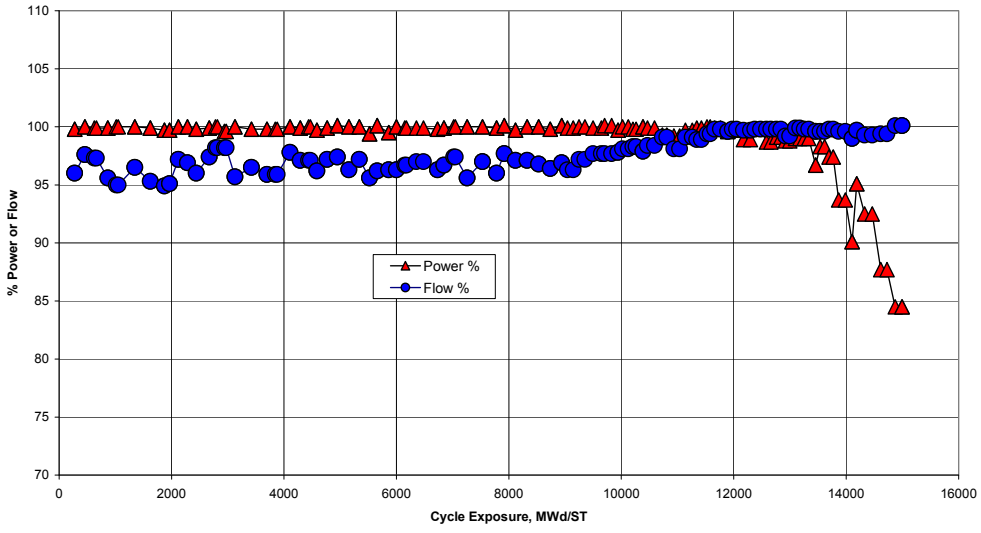

Figure 2.3-2. Power and Flow as a Function of Exposure Cycle 16

2.4 CYCLE 17 OPERATION

Cycle 17 started on 11/01/2004 and ended 10/08/2006. The inventory of fuel in the core is provided in Table 2.4-1. The location of bundles JLD505 and JLM420 in Cycle 17 are provided in Figure 2.4-1. A series of 79 off-line core-tracking cases deplete the core to a cycle average exposure of 15,754.33 MWd/ST at EOC17. At the end of the cycle, all control blades were withdrawn. Figure 2.4-2 provides the power and flow conditions for Cycle 17.

TIP comparisons of the off-line non-adapted model with the measured TIPs are provided in Appendix A.

Table 2.4-1

Bundle Inventory Cycle 17

Bundle Name	IAT	# in Core	#Fresh	Avg Exp GWd/ST
[[	1	180	180	0.00
	2	24	24	0.00
	16	40	0	32.07
	17	112	0	33.27
	18	8	0	29.18
	19	120	0	19.48
]]	20	76	0	18.10
	Total	560	204	15.99

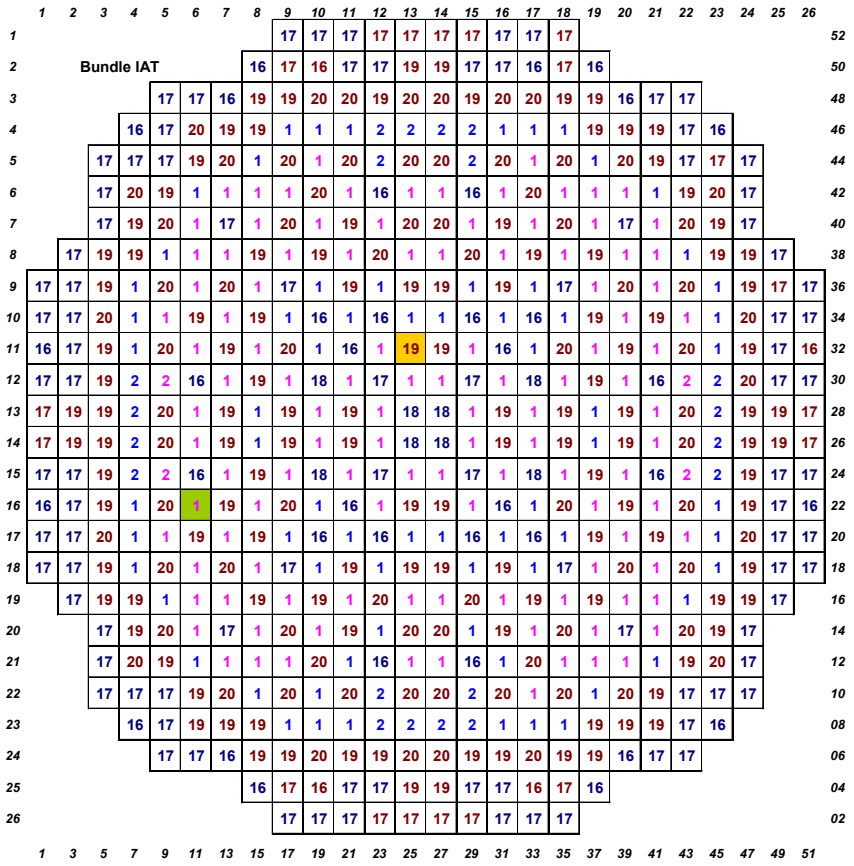

Figure 2.4-1. Core Bundle Type Map Cycle 17

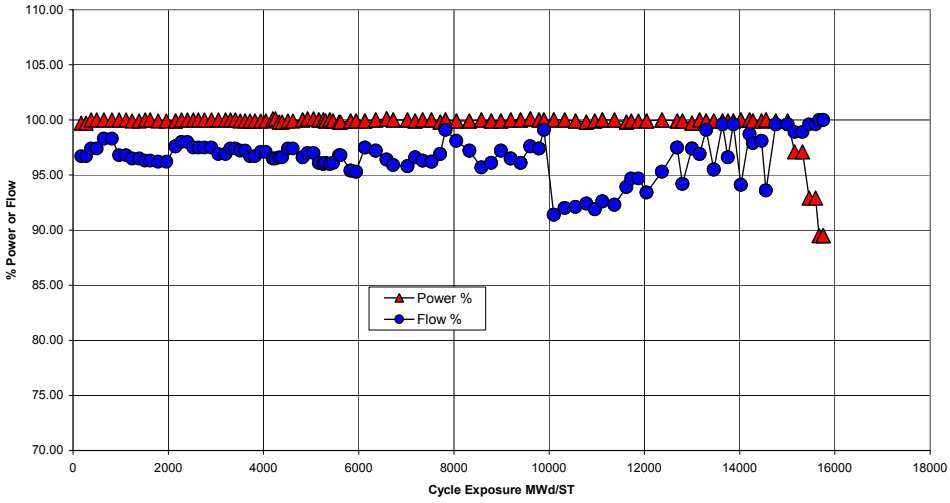

Figure 2.4-2. Power and Flow as a Function of Exposure Cycle 17

2.5 KEY OPERATING PARAMETERS

The Safety Evaluation (SE) by the NRC that covers the Licensing Topical Report NEDC-33173P, "Applicability of GE Methods to Expanded Operating Domains,", Reference [8], discusses "Key Operating Parameters" in Section 2.1.1 of the SE. A portion of this section is paraphrased below.

2.6 SECTION 2.1.1 OF SE

The core thermal-hydraulic conditions for operation at EPU and MELLLA+ can be measured by review of the following key parameters:

(1) Power of Peak Bundle

The bundle power (in MW) is a fundamental direct input to the critical power ratio (CPR) safety parameter calculation, the linear heat generation rate (LHGR), the initial conditions for loss-of-coolant accident (LOCA) response, and the calculation of other intermediate quantities. It represents a local metric of operating conditions and is relevant particularly to the performance of the steady-state nuclear methods.

(2) Coolant Flow for Peak Bundle

The active bundle flow (in Mlbm/hr) is also a direct input to the calculation of the CPR safety parameter, as well as other intermediate quantities.

(3) Exit Void Fraction for Peak Power Bundle

The void fraction results from the integration of the bundle power and flow, as well as the axial distribution of power deposition along the bundle.

(4) Maximum Channel Exit Void Fraction

The peak power bundle (hot channel) may not always coincide with the bundle with the highest channel exit void fraction, since this parameter is based not only on total bundle power, but also on bundle flow.

(5) Core Average Exit Void Fraction

The core average exit void fraction is a core-wide metric on the amount of heat being carried by the coolant.

(6) Peak LHGR

The peak LHGR (in kW/ft) is a reasonable measure of degree of peaking in the core since it is comprised of the combination of radial, axial, and local (pin) power peaking. It is also a key design constraint and monitoring parameter.

(7) Peak Nodal or Pin Exposure

The nodal and pellet exposures are determined by integration of the energy extracted from the local physical area of the fuel given its original specific mass.

2.7 CHARACTERIZATION OF OPERATING CONDITIONS - GAMMA SCAN BUNDLES

The purpose for this section is to characterize some of the operating parameters for the bundles used in the FitzPatrick gamma scan. The following information is based on the non-adapted off-line core tracking.

- Figure 2.7-1. provides information regarding the bundle power (expressed in MWt) as a function of Cycle 7 exposure.
- Figure 2.7-2. provides information regarding the ratio (bundle power in MWt) / (bundle flow in lb/hr) as a function of Cycle 7 exposure.
- Figure 2.7-3. provides information regarding the exit void fraction for the two gamma scan fuel assemblies as a function of Cycle 7 exposure.
- Figure 2.7-4. provides information regarding the bundle peak Linear Heat Generation Rate (LHGR) in kW/ft as a function of Cycle 7 exposure. The LHGR limit is a function of nodal exposure. The kW/ft at the node of Maximum Fraction of Limiting Power Density (MFLPD) is plotted as well as the peak kW/ft for the core and the maximum kW/ft for each of the two gamma scanned fuel bundles.

[[

]]

Figure 2.7-1. Maximum Bundle Power in MWt vs. Cycle 7 Exposure

[[

]]

Figure 2.7-2. Maximum Power / Flow Ratio vs. Cycle 7 Exposure

[[

]]

Figure 2.7-3. Exit Void Fraction vs. Cycle 7 Exposure

[[

]]

Figure 2.7-4. Peak LGHR vs. Cycle 7 Exposure

2.8 DEPLETION HISTORY BUNDLES JLM420 AND JLD505

Bundle JLM420 was loaded in PANACEA location (06,16) in Cycle 17. At the end of cycle 17:

- The Cycle incremental exposure was 15,754.3 MWd/ST.
- The bundle average exposure for bundle JLM420 was 20,736.5 MWd/ST.
- The maximum nodal exposure seen on this bundle was [[ ]] MWd/ST.

Bundle JLD505 was loaded in PANACEA location (12,08) in Cycle 16 and in (13,11) in Cycle 17. At the end of cycle 17:

- The Cycle incremental exposure was 15,754.3 MWd/ST.
- The bundle average exposure for bundle JLD505 was 38,119.4 MWd/ST.
- The maximum nodal exposure seen on this bundle was [[ ]] MWd/ST.

The maximum values seen in power and void fraction are summarized in Table 2.8-1. (These values are the maximum value seen in any of the off-line non-adapted core tracking cases, for Cycle 17 for JLM420 and for Cycles 16 and 17 for bundle JLD505).

The bundle average void fraction and the void fraction in the top node are provided in the following four figures:

- Figure 2.8-1. Bundle JLM420 Void Fractions and Adjacent Rod Position
- Figure 2.8-2. Bundle JLM420 kW/ft and Adjacent Rod Position
- Figure 2.8-3. Bundle JLD505 Void Fractions and Adjacent Rod Position
- Figure 2.8-4. Bundle JLD505 kW/ft and Adjacent Rod Position

Note that the “Max Nodal Power Density” and “Max Bundle kW/ft” values in these figures are specifically those for the nodes at which gamma scan measurements were made.

Table 2.8-1

Maximum Values in Cycles 16 and 17

Bundle	Core Average Power Density kW/L	Max Nodal Power Density kW/L (1)	Max Bundle Average Void Fraction	Max Exit Void Fraction	Max Bundle kW/ft (1)	Max Bundle Radial Power Peaking
JLM420	51.2	[[				]]
JLD505	51.2	[[				]]

(1) Maximum Value Seen for Gamma Scanned Bundles

[[

Figure 2.8-1. Bundle JLM420 Void Fractions and Adjacent Rod Position

[[

]]

Figure 2.8-2. Bundle JLM420 kW/ft and Adjacent Rod Position

[[

]]

Figure 2.8-3. Bundle JLD505 Void Fractions and Adjacent Rod Position

[[

]]

Figure 2.8-4. Bundle JLD505 kW/ft and Adjacent Rod Position

2.9 EOC17 INFORMATION

The following plots provide insights as to the nodal exposure, nodal power, and nodal void fractions seen at EOC17:

- Figure 2.9.1. EOC17 Nodal Exposures for Bundles JLM420 and JLD505
- Figure 2.9.2. EOC17 Nodal Powers for Bundles JLM420 and JLD505
- Figure 2.9.3. EOC17 Nodal Void Fractions for Bundles JLM420 and JLD505

Vertical red lines denote the axial heights at which gamma scan measurements were made.

[[

]]

Figure 2.9.1. EOC17 Nodal Exposures for Bundles JLM420 and JLD505

[[

Figure 2.9.2. EOC17 Nodal Powers for Bundles JLM420 and JLD505

[[

]]

Figure 2.9.3. EOC17 Nodal Void Fractions for Bundles JLM420 and JLD505

3. BUNDLE MEASUREMENTS

3.1 WATER SUBMERSIBLE GAMMA SPECTROMETER

The Water Submersible Gamma Spectrometer (WSGS) measures gamma emissions from individual irradiated fuel rods or individual irradiated fuel bundles in the plant spent fuel pool. Figure 3.1-1 identifies the various components of the WSGS, while Figure 3.1-2 shows the WSGS deployed in the FitzPatrick spent fuel pool.

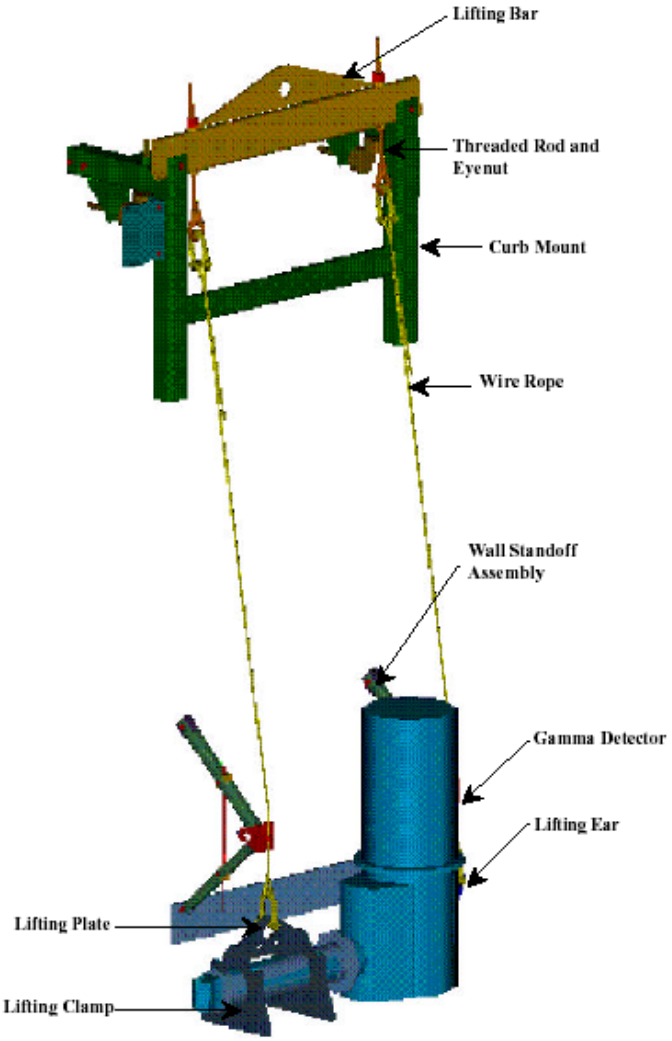

Figure 3.1-1. Components of The Water Submersible Gamma Spectrometer

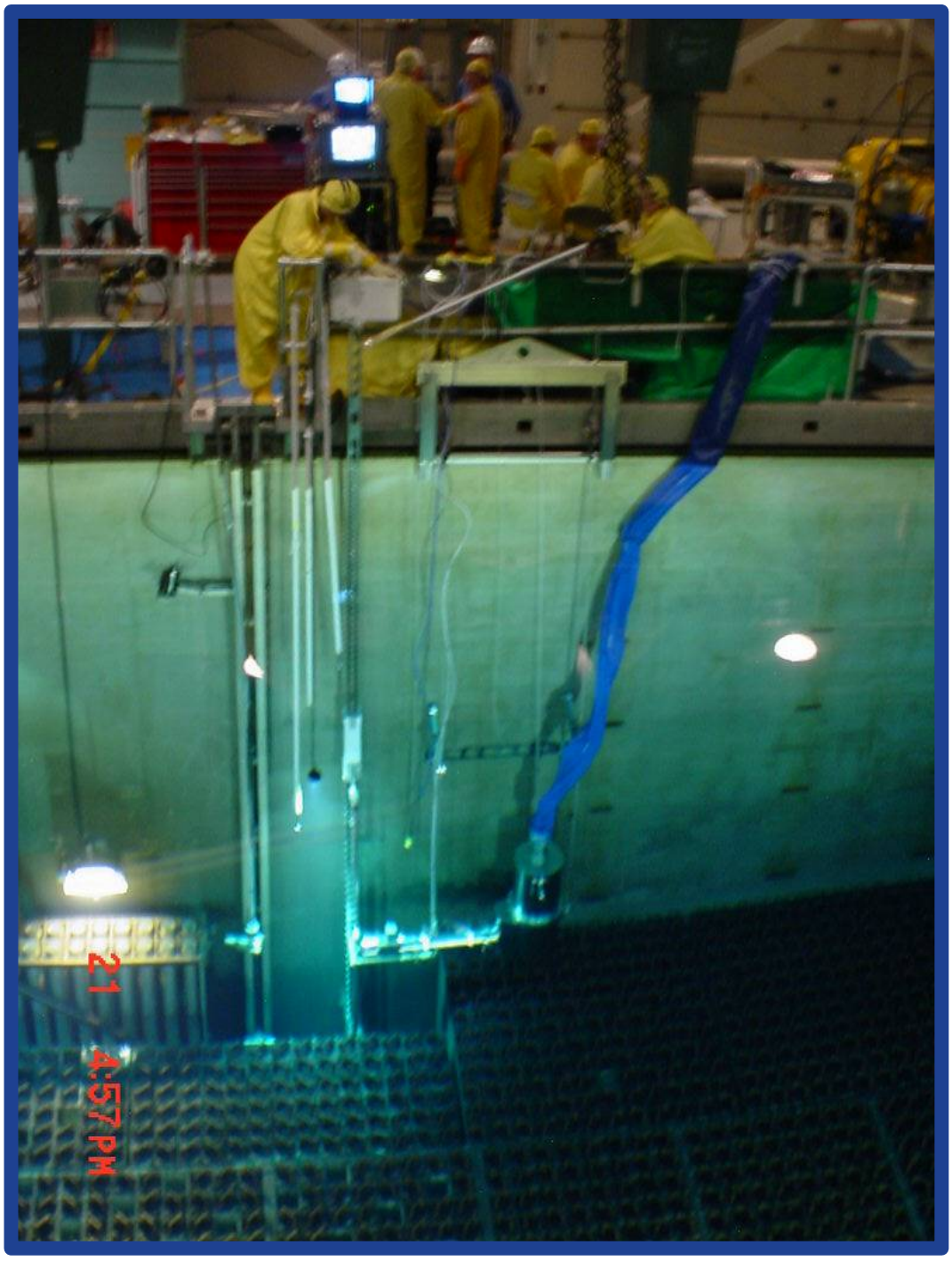

Figure 3.1-2. Deployment of the WSGS at FitzPatrick

3.2 MEASUREMENT DETAILS

For the once-burnt bundle JL420, measurements at 11 axial elevations for [[ ]] different fuel rods were made. Multiple measurements were made on the "reference" rod and on the "weak" rod. A total of [[ ]] separate rod measurements were made

For the reference rod, including four measurements for potential azimuthal dependencies in the measurements, a total of [[ ]] rod measurements were made. There were also [[ ]] measurements of the weak rod. [[ ]]

A total of [[ ]] pin measurements were made.

For the twice-burnt bundle JLD505, again measurements at 11 axial elevations for [[ ]] different fuel rods were planned, for a total of [[ ]] separate rod measurements had been made on [[ ]] rods. By the end of the campaign, [[ ]] rod measurements had been made because of the need to repeat measurements that had larger experimental counting uncertainties.

The first [[ ]] measurements were made with identical conditions to JLM420; with the exception of, new calibrations used with a new detector. After the first [[ ]] measurements, experimental difficulties were compensated for with a slight reconfiguration of the scanner while maintaining reference rod repeat measurements.

[[

]].

A total of [[ ]] pin measurements were determined to be acceptable for use.

4. DESIGN CALCULATIONS

This document provides summaries of the comparisons of design calculations of ^{140}Ba with measured ^{140}La as a means of demonstrating the GNF capabilities for calculating nodal pin powers. There are three analytic approaches summarized herein for predicting the pin-by-pin ^{140}Ba. These include:

- The standard off-line TGBLA06 / PANAC11 non-adapted models used in GNF applications for reload design and licensing (off-line);
- The standard on-line TGBLA06 / PANAC11 application used in 3DMonicore™ with TIP and LPRM shape adaptation for on-line monitoring (adapted off-line); and also
- The use of the lattice code TGBLA06 for nodal depletions, where the operating conditions provided as inputs to the lattice code are derived from the off-line non-adapted (nodal depletions).

For the first two analytic approaches, the pin-by-pin power distributions from the PANAC11 core tracking are post processed to produce the pin-by-pin ^{140}Ba distributions as described in Section 4.1 of Reference [4].

In the third approach, the pin-by-pin ^{140}Ba distributions are obtained directly from the pin-by-pin depletions in the lattice code TGBLA06.

4.1 STATISTICAL COMPARISONS

Comparisons between the (normalized) predicted ^{140}Ba pin-by-pin distributions with the (normalized) measured ^{140}La distributions demonstrate that the uncertainties in the predictions are significantly less than the uncertainties used for pin-by-pin power distributions in the GNF calculation process used in support of licensing calculations.

5. TRADITIONAL BASIS FOR GAMMA SCAN COMPARISONS

In previous GE pin-by-pin Gamma scans, repeat measurements on a reference rod during the course of the experiment were used as a statistical approach to include an evaluation of the uncertainty in the measurements to correct the measured standard deviation. This section provides comparisons of the FitzPatrick measurements to design calculations using this "traditional" approach. Section 6 will use alternate statistical presentation more in line with that used for TIP comparisons.

5.1 DUANE ARNOLD GAMMA SCAN

The most recent GE system gamma scan was performed at the Duane Arnold site in 1987. Individual pin-by-pin gamma scans were performed on a "1984 Lead Test Assembly", an 8x8 bundle with four part length rods. The statistical analysis is based on calculating the ratio of {(predicted / measured)-1} and then forming the standard deviation of this value. In this traditional process, the pin-by-pin values for each axial plane are separately normalized to an average value of 1.0. A series of repeat measurements of a "Reference Rod" at each axial elevation provides information regarding the uncertainty of the measurement process (termed "Measurement Reproducibility"). Table 5.1-1 summarizes the Duane Arnold gamma scan. The [[ ]] standard deviation value provides a reasonable target for the current gamma scan campaign; the intent of the current campaigns is to validate the pin power uncertainties used in the SLMCPR Limit evaluation process.

[[

]]

Table 5.1-1

Duane Arnold Gamma Scan Results

Height from BAZ	Std Dev (TGBLA/Meas)-1 (Comparison Std Dev)	Std Dev Measurement Reproducibility	Corrected Std Dev
[[			
			]]

5.2 SUMMARY – BUNDLE JLM420 – TRADITIONAL BASIS

For the once-burnt bundle JL420, measurements at 11 axial elevations for [[ ]] different fuel rods were made. Multiple measurements were made on the "reference" rod and on the weak rod. There are a number of potential comparisons to design tools that are possible. Pin-by-pin measurements of ^{140}La at multiple axial heights are made. The design tools are then used to predict the Barium distribution, and the measured and predicted distributions are compared. The first set of comparisons use the PANAC11 and post-processing programs to predict the pin-by-pin Barium distributions.

Within this context, there are various models that might be used within this combination of programs. These include two modes of PANACEA usage: (a) non-adapted off-line PANAC11, (b) TIP and LPRM shape adapted (on-line) PANAC11; both of these models use pin power reconstructed local peaking.

The pin-by-pin comparison statistics can be organized by treating (i.e., normalizing) each X-Y plane of the fuel assembly individually (similar to the calculation of local peaking in the infinite lattice TGBLA06 calculation), or by normalizing to the full set of measured data. In the summary tables in this section, the standard deviation of the quantity {(Predicted ^{140}Ba / Measured ^{140}La) –1} is reported, corrected for the measurement reproducibility of the reference rod (1.37%). The traditional measure has been the standard deviation normalized to each X-Y plane; a value of [[ ]] is comparable to the best of the historical pin-by-pin gamma scan measurements. Comparisons for bundle JLM420 are summarized in the following tables. Note that BAZ is the Bottom of the Active Zone.

Results for Bundle JLM420 are provided in the following tables:

- Table 5.2-1 Results for Adapted Off-line – Bundle JLM420
- Table 5.2-2 Results for Non-Adapted Off-line – Bundle JLM420
- Table 5.2-3 Results for TGBLA06 Nodal Depletions – Bundle JLM420

The results for the non-adapted core tracking are remarkably similar to the adapted off-line cases. This is of course because the effects of the axial shape differences are removed by the application of the traditional comparison process.

Note that the number of axial nodes considered for the nodal depletion cases (nine) is smaller than considered for the PANAC11 adapted and non-adapted cases. (The two averaged nodes were not considered in the TGBLA06 analysis).

Table 5.2-1

Results for Adapted Off-line – Bundle JLM420

Height from BAZ (in.)	**Std Dev {(P11/Meas)-1} (Comparison Std Dev)**	**Std Dev of [[ ]] Measurements of Rod [[ ]] (Measurement Reproducibility)**	**Corrected Std Dev**
[[			
			]]

Table 5.2-2

Results for Non-Adapted Off-line – Bundle JLM420

Height from BAZ (in.)	Std Dev {(P11/Meas)-1} (Comparison Std Dev)	Std Dev of [[ ]] Measurements of Rod [[ ]] (Measurement Reproducibility)	Corrected Std Dev
[[			
			]]

Table 5.2-3

Results for TGBLA06 Nodal Depletions – Bundle JLM420

Node	Height from BAZ (in.)	Std Dev {(TGBLA/Meas)-1} (Comparison Std Dev)	Std Dev of [[ ]] Measurements of Rod [[ ]] (Measurement Reproducibility)	Corrected Std Dev TGBLA06 Infinite Lattice Nodal Core Tracking
[[				
				]]

5.3 SUMMARY – BUNDLE JLD505 – TRADITIONAL BASIS

For bundle JLD505, [[ ]] measurements were planned for [[ ]] rods. By the completion of the experiment, [[ ]] measurements had been made on [[ ]] rods. The first [[ ]] measurements were performed with an identical geometrical arrangement as was used on the first bundle, JLM420. After the first [[ ]] measurements on bundle JLD505, experimental difficulties resulted in a slight reconfiguration. The counting characteristics of the two sets of measurements were different.

[[

]].

Results for Bundle JLD505 are provided in the following tables:

- Table 5.3-1- Results for Adapted Off-line – Bundle JLD505
- Table 5.3-2- Results for Non-Adapted Off-line – Bundle JLD505
- Table 5.3-3- Results for TGBLA06 Nodal Depletions – Bundle JLD505

Table 5.3-1

Results for Adapted Off-line – Bundle JLD505

Height from BAZ (in.)	**Std Dev {(P11/Meas)-1} (Comparison Std Dev)**	**Std Dev of [[ ]] Measurements of Rod [[ ]] (Measurement Reproducibility)**	**Corrected Std Dev**
[[			
			]]

Table 5.3-2

Results for Non-Adapted Off-line – Bundle JLD505

Height from BAZ (in.)	Std Dev {(P11/Meas)-1} (Comparison Std Dev)	Std Dev of [[ ]] Measurements of Rod [[ ]] (Measurement Reproducibility)	Corrected Std Dev
[[			
			]]

Table 5.3-3

Results for TGBLA06 Nodal Depletions – Bundle JLD505

Node	Height from BAZ (in.)	Std Dev {(TGBLA/Meas)-1} (Comparison Std Dev)	Std Dev of [[ ]] Measurements of Rod [[ ]] (Measurement Reproducibility)	Corrected Std Dev TGBLA06 Infinite Lattice Nodal Core Tracking
[[				
				]]

5.4 DETAILS OF TRADITIONAL COMPARISONS – NODAL DEPLETIONS

This section will provide more details on one of the three analytic comparisons (the TGBLA06 nodal depletions).

5.4.1 Bundle JLM420 – Nodal Depletions

In the following figures, various sets of data for bundle JLM420 are provided on a pin-by-pin basis (normalized measured ^{140}La, normalized predicted ^{140}Ba, and (Predicted/Measured) -1. These two-dimensional data will be provided for the nine different axial elevations for which TGBLA06 nodal depletions were developed. In the following figures, the measured ^{140}La decay corrected count rate data is normalized so that the average value is 1.0 for each XY slice at each elevation

The color code for this presentation of the data is supplied in Figure 5.4.1-1.

The following figures provide the measured ^{140}La data, the predictions of ^{140}Ba using the TGBLA nodal depletion process, and the pin-by-pin comparisons between measured ^{140}La and predicted ^{140}Ba:

- Figure 5.4.1-2. Measured Normalized ^{140}La for Bundle JLM420 (93 in. to 123 in.)
- Figure 5.4.1-3. Measured Normalized ^{140}La for Bundle JLM420 (27 in. to 87 in.)
- Figure 5.4.1-4. TGBLA Predicted Normalized ^{140}La for Bundle JLM420 (93 in. to 123 in.)
- Figure 5.4.1-5. TGBLA Predicted Normalized ^{140}La for Bundle JLM420 (27 in. to 87 in.)
- Figure 5.4.1-6. Pin-by-Pin {(TGBLA/Meas)-1} For Bundle JLM420 (93 in. to 123 in.)
- Figure 5.4.1-7. Pin-by-Pin {(TGBLA/Meas)-1} For Bundle JLM420 (27 in. to 87 in.)

[[

]]

Figure 5.4.1-1. Color Code For XY Lattice Data

[[

]]

Figure 5.4.1-2. Measured Normalized ^{140}La for Bundle JLM420 (93 in. to 123 in.)

[[

]]

Figure 5.4.1-3. Measured Normalized ^{140}La for Bundle JLM420 (27 in. to 87 in.)

[[

Figure 5.4.1-4. TGBLA Predicted Normalized ^{140}La for Bundle JLM420 (93 in. to 123 in.)

[[

]]

Figure 5.4.1-5. TGBLA Predicted Normalized ^{140}La for Bundle JLM420 (27 in. to 87 in.)

[[

Figure 5.4.1-6. Pin-by-Pin {(TGBLA/Meas)-1} For Bundle JLM420 (93 in. to 123 in.)

[[

Figure 5.4.1-7. Pin-by-Pin {(TGBLA/Meas)-1} For Bundle JLM420 (27 in. to 87 in.)

5.4.2 Bundle JLD540 – Nodal Depletions

In the following figures, various sets of data for bundle JLD505 are provided on a pin-by-pin basis (normalized measured ^{140}La, normalized predicted ^{140}Ba, and {(Predicted/Measured) –1}. These two-dimensional data will be provided for the nine different axial elevations for which TGBLA06 nodal depletions were developed. In the following figures, the measured ^{140}La decay corrected count rate data is normalized so that the average value is 1.0 for each XY slice at each elevation.

The color code for this presentation of the data is supplied in Figure 5.4.2-1.

The following figures provide the measured ^{140}La data, the predictions of ^{140}Ba using the TGBLA nodal depletion process, and the pin-by-pin comparisons between measured ^{140}La and predicted ^{140}Ba:

- Figure 5.4.2-2. Measured Normalized ^{140}La for Bundle JLD505 (93 in. to 123 in.)
- Figure 5.4.2-3. Measured Normalized ^{140}La for Bundle JLD505 (27 in. to 87 in.)
- Figure 5.4.2-4. TGBLA Predicted Normalized ^{140}La for Bundle JLD505 (93 in. to 123 in.)
- Figure 5.4.2-5. TGBLA Predicted Normalized ^{140}La for Bundle JLD505 (27 in. to 87 in.)
- Figure 5.4.2-6. Pin-by-Pin {(TGBLA/Meas)-1} For Bundle JLD505 (93 in. to 123 in.)
- Figure 5.4.2-7. Pin-by-Pin {(TGBLA/Meas)-1} For Bundle JLD505 (27 in. to 87 in.)

[[

]]

Figure 5.4.2-1. Color Code For XY Lattice Data

[[

]]

Figure 5.4.2-2. Measured Normalized ^{140}La for Bundle JLD505 (93 in. to 123 in.)

[[

]]

Figure 5.4.2-3. Measured Normalized ^{140}La for Bundle JLD505 (27 In. to 87 In.)

[[

]]

Figure 5.4.2-4. TGBLA Predicted Normalized ^{140}La for Bundle JLD505 (93 in. to 123 in.)

[[

]]

Figure 5.4.2-5. TGBLA Predicted Normalized ^{140}La for Bundle JLD505 (27 in. to 87 in.)

[[

]]

Figure 5.4.2-6. Pin-by-Pin {(TGBLA/Meas)-1} For Bundle JLD505 (93 in. to 123 in.)

[[

]]

Figure 5.4.2-7. Pin-by-Pin {(TGBLA/Meas)-1} For Bundle JLD505 (27 in. to 87 in.)

6. PIN NODAL, BUNDLE, AND AXIAL ROOT MEAN SQUARE (RMS) COMPARISONS

The traditional comparison process provides insights as to the comparison of pin-by-pin power distribution within an X-Y plane, but the axial shape of the comparison is eliminated from consideration by the normalization process.

This section provides a different view of the comparison process, analogous to the techniques common to the TIP comparison process. Similar to the TIP comparison process, the following three quantities are evaluated and compared:

- Pin Nodal RMS
- Rod RMS
- Axial Average RMS

In these comparisons, all measurements at all elevations are normalized to a value of 1.0. The Pin Nodal RMS evaluations provide insights as to the ability of the code packages to calculate the fuel rod kW/ft for a particular height of a particular fuel rod. The Rod RMS evaluations provide insights as to the ability of the code package to calculate the axially integrated fuel rod power. The axial average RMS evaluation provides insights as to the accuracy with which the bundle average axial power distribution is calculated.

As contrasted with the TIP comparison process (See Appendix A), however, where all TIP strings have the same number of measurements, it is noted that not all rods that are gamma scanned in the fuel assembly are measured for ^{140}La, and the number of measurements finally obtained for each rod j may be different. For example, for part length rods there will be fewer measurements than for full-length rods. Also, for various reasons, there may not be measurements finally available for all axial elevations of all rods. Some data at a particular elevation may be missing, or the experimental counting uncertainties may be too large, causing the data for this measurement to be eliminated.

6.1 DESCRIPTION OF STATISTICS

6.1.1 Definitions

Let:

M(k, j) = Normalized Measured ^{140}La at axial elevation k for rod j

C(k, j) = Normalized Calculated ^{140}Ba at axial elevation k for rod j

K(j)= Number of axial measurements for rod j

J = Number of rods for which measurements are available for this fuel assembly

The measured ^{140}La and calculated ^{140}Ba are normalized in the same manner, as follows:

[[

]]

6.1.2 Pin Nodal RMS

[[ ]]

6.1.3 Rod RMS

[[ ]]

6.1.4 Axial Average RMS

[[ ]]

6.2 PIN NODAL, ROD AVERAGED, AND AXIAL AVERAGE STATISTICAL SUMMARY

The pin nodal, rod averaged, and axial average statistics for each of the three analytical comparisons for the two bundles gamma scanned at FitzPatrick are provided below. As will be seen later, the TIP comparisons (Off-line non-adapted calculated TIPS compared to measured TIPs) will document a cycle average of [[ ]] nodal RMS value (with [[ ]] for the end of cycle TIP comparison). This TIP value represents (more or less) a result averaged over the four bundles surrounding the TIP string. This compares to the gamma scan values of between [[ ]] for the pin nodal RMS.

Thus the pin nodal gamma scan results are of the same order of magnitude of the TIP comparisons, and the gamma scan and the TIP results are consistent and complement each other. Note that the statistics presented in the following three tables are for each bundle separately.

- Table 6.2-1. Pin Nodal, Rod Averaged, and Axial Average Statistical Summary – Adapted Off-line
- Table 6.2-2. Pin Nodal, Rod Averaged, and Axial Average Statistical Summary – Off-line
- Table 6.2-3. Pin Nodal, Rod Averaged, and Axial Average Statistical Summary – Nodal Depletions

Table 6.2-1.

Pin Nodal, Rod Averaged, and Axial Average Statistical Summary – Adapted Off-line

Bundle	Pin Nodal RMS	Rod Averaged RMS	Axial Averaged RMS
JLM420	[[		
JLD505			]]

Table 6.2-2.

Pin Nodal, Rod Averaged, and Axial Average Statistical Summary Off-line

Bundle	Pin Nodal RMS	Rod Averaged RMS	Axial Averaged RMS
JLM420	[[		
JLD505			]]

Table 6.2-3.

Pin Nodal, Rod Averaged, and Axial Average Statistical Summary – Nodal Depletions

Bundle	Pin Nodal RMS	Rod Averaged RMS	Axial Averaged RMS
JLM420	[[		
JLD505			]]

6.3 SUMMARY PLOTS OF PIN NODAL RMS

6.3.1 Summary Plot for Adapted Off-line – Pin Nodal RMS

This section provides a comparison of the normal on-line TIP and LPRM-adapted design tools with the results of the gamma scan. This case is generated with TIP and LPRM shape adapted PANAC11 core tracking. This adapted off-line core tracking reproduces the thermal limits seen in the on-line monitoring. Figure 6.3.1-1. combines the results of the prediction of ^{140}Ba generated with PANAC11 for both measured bundles versus the measured ^{140}La.

The RMS value for this comparison is [[ ]]. This value represents the combined RMS value for both bundles. In Figure 6.3.1-1., the predicted ^{140}Ba is the normalized predicted ^{140}Ba number density from TGBLA06 for that particular rod, and the measured ^{140}La is the normalized measured decay corrected count rates for ^{140}La. Both predicted and measured values are normalized to an average value of 1.0.

[[

]]

Figure 6.3.1-1. Combined Pin Nodal RMS for Bundles JLM420 and JLD505 for Adapted Off-line

6.3.2 Summary Plot for Off-line – Pin Nodal RMS

This comparison provides a summary of the off-line non-adapted results with the gamma scan measurements. Figure 6.3.2-1 combines the results of the prediction of ^{140}Ba generated for both measured bundles versus the measured ^{140}La.

The RMS value for this comparison is [[ ]]. This value represents the combined RMS value for both bundles. [[

]]. Again, both predicted and measured values are normalized to an average value of 1.0.

[[

]]

Figure 6.3.2-1. Combined Pin Nodal RMS for Bundles JLM420 and JLD505 for Off-line

6.3.3 Summary Plot for Nodal Depletions – Pin Nodal RMS

This case provides a comparison of the use of the lattice code TGBLA06 to compute the predicted ^{140}Ba (generated by replicating the nodal tracking from the PANAC11 off-line core tracking with the lattice code) with the gamma scan measurements. In this approach the nodal PANAC11 values for power density, void fraction, and control rod presence are used in the TGBLA06 code to deplete to the end of cycle. Figure 6.3.3-1. combines the results of the prediction of ^{140}Ba generated with TGBLA06 for both measured bundles versus the measured ^{140}La.

The RMS value for this comparison is [[ ]]. This value represents the combined RMS value for both bundles.

[[

]]

Figure 6.3.3-1. Combined Pin Nodal RMS for Bundles JLM420 and JLD505 for Nodal Depletions

6.4 SUMMARY OF ROD AVERAGED RMS COMPARISONS

6.4.1 Rod Averaged RMS Comparisons for Adapted Off-line

Figures 6.4.1-1. and 6.4.1-2. compare the measured ^{140}La and predicted ^{140}Ba distributions on a rod-by-rod basis for the two gamma scanned bundles. In these figures, the "radial" value is derived by first calculating the "average" value of the (normalized to 1.0 over all measurements) ^{140}La measured for that fuel rod. The average value of ^{140}Ba predicted for that same number of axial elevations is then computed. Corner rods (tan), rods next to corner rods (grey), water rods (yellow), and gadolinium rods (green) are color coded in the lattice map. For bundle JLM420:, the rod average RMS value is [[ ]]. For bundle JLD505, the rod average RMS value is [[ ]].

[[

]]

Figure 6.4.1-1. Rod Averaged RMS for Bundle JLM420 Adapted Off-line

[[

]]

Figure 6.4.1-2. Rod Averaged RMS for Bundle JLD505 Adapted Off-line

6.4.2 Rod Averaged RMS Comparisons for Off-line

Figures 6.4.2-1. and 6.4.2-2. compare the measured ^{140}La and predicted ^{140}Ba distributions on a rod-by-rod basis for the two gamma scanned bundles for the Off-line core tracking process. Corner rods (tan), rods next to corner rods (grey), water rods (yellow), and gadolinium rods (green) are color coded in the lattice map. For bundle JLM420 the rod average RMS value is [[ ]]. For bundle JLD505 the rod average RMS value is [[ ]].

[[

]]

Figure 6.4.2-1. Rod Averaged RMS for Bundle JLM420 Off-line

[[

]]

Figure 6.4.2-2. Rod Averaged RMS for Bundle JLD505 Off-line

6.4.3 Rod Averaged RMS Comparisons for Nodal Depletions

Figures 6.4.3-1. and 6.4.3-2. compare the measured ^{140}La and predicted ^{140}Ba distributions on a rod-by-rod basis for the two gamma scanned bundles for the TGBLA nodal depletion process. Corner rods (tan), rods next to corner rods (grey), water rods (yellow), and gadolinium rods (green) are color coded in the lattice map. For bundle JLM420, the rod average RMS value is [[ ]]. For bundle JLD505, the rod average RMS value is [[ ]].

[[

]]

Figure 6.4.3-1. Rod Averaged RMS for Bundle JLM420 Nodal Depletion

[[

]]

Figure 6.4.3-2. Rod Averaged RMS for Bundle JLD505 Nodal Depletion

6.5 SUMMARY OF AXIAL AVERAGED RMS COMPARISONS

6.5.1 Axial Averaged RMS Comparisons for Adapted Off-line

Figures 6.5.1-1. and 6.5.1-2. compare the axial averaged predicted ^{140}Ba and the measured ^{140}La for the TIP and LPRM adapted case. For bundle JLM420, the axial RMS value is [[ ]]. For bundle JLD505, the axial RMS value is [[ ]].
[[

]]

Figure 6.5.1-1. Axial Averaged RMS for Bundle JLM420 Adapted Off-line

[[

]]

Figure 6.5.1-2. Axial Averaged RMS for Bundle JLD505 Adapted Off-line

6.5.2 Axial Averaged RMS Comparisons for Off-line

Figures 6.5.2-1. and 6.5.2-2. compare the axial averaged predicted ^{140}Ba and the measured ^{140}La for the off-line case (i.e., non-adapted off-line core tracking). For bundle JLM420, the axial RMS value is [[ ]]. For bundle JLD505, the axial RMS value is [[ ]].

[[

]]

Figure 6.5.2-1. Axial Averaged RMS for Bundle JLM420 Off-line

[[

]]

Figure 6.5.2-2. Axial Averaged RMS for Bundle JLD505 Off-line

6.5.3 Axial Averaged RMS Comparisons for Nodal Depletion

Figures 6.5.3-1. and 6.5.3-2. compare the axial averaged predicted ^{140}Ba and the measured ^{140}La for the TGBLA nodal depletion case. For bundle JLM420, the axial RMS value is [[ ]]. For bundle JLD505, the axial RMS value is [[ ]].
[[

]]

Figure 6.5.3-1. Axial Averaged RMS for Bundle JLM420 Nodal Depletion

[[

]]

Figure 6.5.3-2. Axial Averaged RMS for Bundle JLD505 Nodal Depletion

7. SUMMARY OF UNCERTAINTIES

7.1 PIN-BY-PIN GAMMA SCAN IMPACT ON UNCERTAINTIES FOR MELLLA+ ANALYSES

As discussed in NEDC-32601P-A (Section 3.1), the uncertainties in pin power peaking factor is a combination of three uncertainty factors, [[

]]

These uncertainties can be combined as summarized in Table 7.1-1.

Table 7.1-1

Components of Pin Power Peaking Uncertainty

Component	NEDC-32601P	NEDC-33173P Table 2-11
[[		
		]]

The "Total Uncertainty" is again calculated using the SRSS.

These uncertainties are evaluated on a lattice basis (that is, for one XY slice of a fuel assembly at any one axial height). The next section compares the measurement / analysis results with these uncertainties.

7.2 SUMMARY OF MEASURED UNCERTAINTIES –PIN-BY-PIN XY

As documented in Sections 5.2 and 5.3, the results of the gamma scan comparisons for all three modeling approaches provide better statistics than the uncertainties summarized in NEDC-32601P-A.

This set of comparisons is based on normalization of the data to 1.0 for each axial level separately. In these comparisons, therefore, the effects of bundle axial and radial power distributions have been removed. These are lattice comparisons, or XY comparisons.

The measured comparison values explicitly include the actual effects of all [[

]]

Table 7.2-1

Comparisons of Pin Power Peaking Measurement Statistics

Bundle	Core Tracking Modeling	Corrected Std Dev
JLM420	Adapted Off-line	[[
JLM420	Off-Line	
JLM420	Nodal Depletion	
JLD505	Adapted Off-line	
JLD505	Off-Line	
JLD505	Nodal Depletion	]]

As shown in Table 7.2-1, the largest uncertainty is [[ ]], which is significantly smaller than the value of [[ ]] from Section 3.1.4 of NEDC-32601P-A.

8. TRENDING AND VISUALIZATION

The purpose for doing the gamma scan measurements is to provide confirmation that the lattice and 3-D steady state models provide reasonable evaluations of key operating thermal margins and power distributions. The experimental data and the comparisons to calculated data may help reveal potential weaknesses in the design process. For this reason, reviewing the data for any trends in the uncertainties in the calculation results is a useful exercise. All trends and information in this section focus on bundle JLM420, the lower exposure fuel assembly.

8.1 TRENDS IN UNCERTAINTIES VS. NODAL PARAMETERS

Section 2.6 discussed some key operating parameters that can be used for characterization of the operating conditions seen for fuel assemblies. In looking for trends, it may be interesting to see if there is any correlation in the accuracy of the design tools with respect to power, void fraction and exposure. Some of the key operating parameters in Section 2.6 reference bundle integral quantities. Here, the measurements regard pin-by-pin information, and the potential for trending in the uncertainty is compared to nodal quantities, not to bundle integral quantities.

No evidence of a dependency (or trend) of the pin-by-pin uncertainties for bundle JLM420 could be identified for the following items:

- Nodal Power
- Nodal Exposure
- Nodal Void Fraction
- Channel Distortion (Channel Bow)

8.2 XYZ PLOTS OF {(TGBLA/MEAS)-1} PIN-BY-PIN ERRORS – BUNDLE JLM420

One method of identifying trends in the uncertainties is to visualize the error in the calculation process. In this discussion, "TGBLA" refers to the normalized pin-by-pin ^{140}Ba predicted by TGBLA06 nodal depletions, and "Measured" refers to the normalized ^{140}La measured in the gamma scan campaign. In Figures 8.2-1. through 8.2-9., the quantity {(TGBLA/Measured)-1} is displayed for each pin at the nine elevations for which TGBLA06 nodal depletions were compared to the measured data. In these figures, the lattice is viewed from the location of the instrument tube – that is, the narrow-narrow corner is nearest the front, and the control rod location would be towards the back of the figure. Each row of fuel pins is assigned a different color in these plots.

[[

]]

[[

]]

Figure 8.2-1. {(TGBLA/Meas)-1} For Bundle JLM420 at 27 In.

[[

]]

Figure 8.2-2. {(TGBLA/Meas)-1} For Bundle JLM420 at 45 In.

[[

]]

Figure 8.2-3. {(TGBLA/Meas)-1} For Bundle JLM420 at 63 In.

[[

]]

Figure 8.2-4. {(TGBLA/Meas)-1} For Bundle JLM420 at 81 In.

[[

]]

Figure 8.2-5. {(TGBLA/Meas)-1} For Bundle JLM420 at 87 In.

[[

]]

Figure 8.2-6. {(TGBLA/Meas)-1} For Bundle JLM420 at 93 In.

[[

]]

Figure 8.2-7. {(TGBLA/Meas)-1} For Bundle JLM420 at 99 In.

[[

]]

Figure 8.2-8. {(TGBLA/Meas)-1} For Bundle JLM420 at 111 In.

[[

]]

Figure 8.2-9. {(TGBLA/Meas)-1} For Bundle JLM420 at 123 In.

8.3 XYZ PLOTS OF {(P11/MEAS)-1} PIN-BY-PIN ERRORS – BUNDLE JLM420 – OFF-LINE ADAPTATION

In Figures 8.3-1. through 8.3-9., the quantity {(P11/Measured)-1} is displayed for each pin at the eleven elevations for which PANAC11 predicted pin-by-pin ^{140}Ba was compared to the measured ^{140} La data. In these figures, the lattice is viewed from the location of the instrument tube – again, the narrow-narrow corner is nearest the front, and the control rod location would be towards the back of the figure.

[[

]].

[[

]]

Figure 8.3-1. {(P11/Meas)-1} For Bundle JLM420 at 27 In.

[[

]]

Figure 8.3-2. {(P11/Meas)-1} For Bundle JLM420 at 45 In.

[[

]]

Figure 8.3-3. {(P11/Meas)-1} For Bundle JLM420 at 63 In.

[[

]]

Figure 8.3-4. {(P11/Meas)-1} For Bundle JLM420 at 81 In.

[[

]]

Figure 8.3-5. {(P11/Meas)-1} For Bundle JLM420 at 87 In.

[[

]]

Figure 8.3-6. {(P11/Meas)-1} For Bundle JLM420 at 90 In.

[[

]]

Figure 8.3-7. {(P11/Meas)-1} For Bundle JLM420 at 93 In.

[[

]]

Figure 8.3-8. {(P11/Meas)-1} For Bundle JLM420 at 99 In.

[[

]]

Figure 8.3-9. {(P11/Meas)-1} For Bundle JLM420 at 102 In.

[[

]]

Figure 8.3-10. {(P11/Meas)-1} For Bundle JLM420 at 111 In.

[[

]]

Figure 8.3-11. {(P11/Meas)-1} For Bundle JLM420 at 123 In.

8.4 POTENTIAL TRENDS [[ ]]

[[

]]

[[

]]

Figure 8.4-1. {(P11/Meas)-1} vs. [[ ]]

[[

]]

Figure 8.4-2. {(P11/Meas)-1} vs. [[ ]]

[[

]]

Figure 8.4-3. {(P11/Meas)-1} vs. [[ ]]

[[

]]

Figure 8.4-4. {(P11/Meas)-1} vs. [[ ]]

8.4.1 Potential Impact [[ ]]

[[

]].

9. REFERENCES

1. Letter from USNRC to G. A. Watford (GE), "Amendment 26 to GE Licensing Topical Report NEDE-24011-P-A, 'GESTAR II' - Implementing Improved GE Steady-State Methods," November 10, 1999.
2. GE Nuclear Energy, “Power Distribution Uncertainties for Safety Limit MCPR Evaluations,” NEDC-32694P-A, August 1999.
3. GE Nuclear Energy, “Advanced Methods Power Distribution Uncertainties for Core Monitoring,” NEDC-32773P, Revision 1, January 1999.
4. GE Hitachi Nuclear Energy, NEDC-33173P, Supplement 2 Part 1, Licensing Topical Report, Applicability of GE Methods to Expanded Operating Domains – Power Distribution Validation for Cofrentes Cycle 13, August 2009.
5. GE Nuclear Energy, “Methodology and Uncertainties for Safety Limit MCPR Evaluations,” NEDC-32601P-A, August 1999.
6. GE Nuclear Energy, Letter, J. S. Post to NRC, Document Control Desk, “Part 21 Evaluation; Power Distribution Uncertainty Reassessment,” MFN05-082, August 18, 2005.
7. GE Nuclear Energy “Applicability of GE Methods to Expanded Operating Domains” NEDC-33173P,” February 2006.
8. Letter from TB Blount (NRC) to JG Head (GEH), Subject: Final Safety Evaluation for GE Hitachi Nuclear Energy Americas, LLC Licensing Topical Report NEDC-33173P, “Applicability Of GE Methods To Expanded Operating Domains” (TAC No. MD0277), July 21, 2009.

Appendix A OFF-LINE NON-ADAPTED TIP COMPARISONS

The definitions of statistics used in these TIP comparisons are provided in the Cofrentes LTR.

A.1 CYCLE 17 NON-ADAPTED TIP SETS

There were only eight TIP sets run during the cycle. These are summarized in Table A.1-1 and Figure A.1-1.

From sometime after April, 2007 until very near the end of cycle in October, 2007, there was apparently a problem with one of the TIP machines. Apparently for these TIPs, the values were not normalized to the same integral value as the TIP data from the other TIP machines. As a result, the nodal RMS difference between the measured and calculated TIPs increased dramatically for the June, 2007 TIP set, as shown in the following table and plots. This problem was apparently corrected by the last TIP set.

A.2 CYCLE 17 - COMPARISON OF CORE AVERAGE AXIAL TIPS – NON-ADAPTED

This subsection provides snapshots of the comparison of the measured and calculated core average axial TIPs at the eight exposure points in Cycle 17. The progression from a more bottom peaked power distribution at the middle of cycle to a more top peaked power distribution at the end of cycle can be inferred from the core average axial TIP plots.

Table A.1-1 Cycle 17 Non-Adapted TIP Sets

Case	Qualifier	MWd/ST	MW(t)	Mlbm/hr	Bundle RMS	Axial RMS	Nodal RMS	Core Avg Ex. Void	Maximum Exit Void
1	FMTS10502031	2288	2537	75.2	[[				
2	FMTD10504281	4210	2534	74.4					
3	FMTD10510211	7838	2536	76.3					
4	FMTD10601121	9735	2535	75.1					
5	FMTD10603161	11160	2530	71.0					
6	FMTD10604111	11753	2535	72.8					
7	FMTD10606271	13473	2531	73.6					
8	FMTS1061006	15754	2271	77.0					
	RMS								
	Mean								
	St. Deviation								
	Minimum								]]

[[

]]

Figure A.1-1. Cycle 17 TIP RMS Values

[[

]]

Figure A.2-1. Axial Average TIP Comparison at 2288 MWd/ST

[[

]]

Figure A.2-2. Individual TIP Comparisons At 2288 MWd/ST

[[

]]

Figure A.2-3. Axial Average TIP Comparison at 4210 MWd/ST

[[

]]

Figure A.2-4. Individual TIP Comparisons At 4210 MWd/ST

[[

]]

Figure A.2-5. Axial Average TIP Comparison at 7838 MWd/ST

[[

]]

Figure A.2-6. Individual TIP Comparisons At 7838 MWd/ST

[[

]]

Figure A.2-7. Axial Average TIP Comparison at 9735 MWd/ST

[[

]]

Figure A.2-8. Individual TIP Comparisons At 9735 MWd/ST

[[

]]

Figure A.2-9. Axial Average TIP Comparison at 11160 MWd/ST

[[

]]

Figure A.2-10. Individual TIP Comparisons At 11160 MWd/ST

[[

]]

Figure A.2-11. Axial Average TIP Comparison at 11753 MWd/ST

[[

]]

Figure A.2-12. Individual TIP Comparisons At 11753 MWd/ST

[[

]]

Figure A.2-13. Axial Average TIP Comparison at 13472 MWd/ST

[[

]]

Figure A.2-14. Individual TIP Comparisons At 13472 MWd/ST

[[

]]

Figure A.2-15. Axial Average TIP Comparison at 15754 MWd/ST

[[

]]

Figure A.2-16. Individual TIP Comparisons At 15754 MWd/ST